Journal of Alloys and Compounds 489 (2010) 13–19

Contents lists available at ScienceDirect

Journal of Alloys and Compounds

journal homepage: www.elsevier.com/locate/jallcom

Magnetic properties and magnetocaloric effect of $Nd(Mn_{1-x}Fe_x)_2Ge_2$ compounds

Y.Q. Chen [a], J. Luo [a,*], J.K. Liang [a,b], J.B. Li [a], G.H. Rao [a]

[a] Beijing National Laboratory for Condensed Matter Physics, Institute of Physics, Chinese Academy of Sciences, Beijing 100190, China
[b] International Center for Materials Physics, Academia Sinica, Shenyang 110016, China

ARTICLE INFO

Article history:
Received 15 August 2009
Received in revised form
10 September 2009
Accepted 15 September 2009
Available online 23 September 2009

Keywords:
Metals and alloys
Magnetocaloric
X-ray diffraction

ABSTRACT

Polycrystalline $Nd(Mn_{1-x}Fe_x)_2Ge_2$ ($0 \le x \le 1$) compounds have been prepared by arc-melting. X-ray powder diffraction analysis shows that all samples crystallize in the $ThCr_2Si_2$-type structure with the space group *I4/mmm*. The substitution of Fe for Mn results in decreases of the lattice constants *a*, *c* and the unit-cell volume *V*. Magnetic properties and magnetocaloric effect of the compounds $Nd(Mn_{0.9}Fe_{0.1})_2Ge_2$ and $Nd(Mn_{0.8}Fe_{0.2})_2Ge_2$ have been studied by magnetic measurements. A spin reorientation transition at about 188 K is observed for $Nd(Mn_{0.9}Fe_{0.1})_2Ge_2$. The $Nd(Mn_{0.8}Fe_{0.2})_2Ge_2$ compound shows more complicated magnetic behavior, which is characterized by four magnetic ordering states below room temperature. The maximum values of the magnetic entropy change are 2.35 and 1.84 J kg^{-1} K^{-1} for $x = 0.1$ and 0.2, respectively, under the applied field changing from 0 to 5 T. The relative cooling powers of $Nd(Mn_{0.9}Fe_{0.1})_2Ge_2$ and $Nd(Mn_{0.8}Fe_{0.2})_2Ge_2$ are 145.9 and 133.8 J kg^{-1} under an applied field change of 5 T.

1. Introduction

Recently, the magnetocaloric effects of magnetic materials receive a great deal of attention in order to identify potential magnetic refrigerants [1–5]. The magnetocaloric effect (MCE) found by Warbury [6] provides a unique way to realize refrigeration from room temperature to ultralow temperatures. With an increase of the applied field, the magnetic entropy decreases and heat is emitted from the magnetic system to the environment in an isothermal process. With a decrease of the applied field, the magnetic entropy increases and heat is absorbed by the magnetic system in an adiabatic process. During the last few years, many rare earth (R)–transition metal (TM) intermetallic compounds have been shown to possess giant MCE [7–10]. Based on the various reports available, it is ascertained that giant MCE can be obtained only in materials showing first-order transitions, magneto-structural transitions or field-induced metamagnetic transitions [11–13]. In order to identify potential refrigerant materials from the reservoir of rare earth (R)–transition metal (TM) intermetallics, many materials are being revisited with regard to their MCE.

Among the R–TM intermetallics, RMn_2X_2 (X = Si, Ge) have attracted a lot of attention due to their interesting magnetic properties [14–17]. Normally, this type of compounds crystallize in the body-centered tetragonal $ThCr_2Si_2$-type structure with the space group *I4/mmm*, in which R, Mn, and X atoms occupy 2a (0,0,0), 4d (0,1/2,1/4) and 4e (0,0,*z*) sites, respectively. The unit cell consists of two formula units and the compound has a layered structure with the sequence ...R-X-Mn_2-X-R-X-Mn_2-X-R... planes (so-called '$BaAl_4$' slab) stacked along the *c*-axis. Consequently, the distances between the atoms mainly depend on the *a*- and *c*-parameters [18], which is favorable to analyze the magnetic properties of these compounds based on the Mn–Mn distance. In this series, both R and Mn atoms possess magnetic moments. It has been reported that in most of the RMn_2X_2 (X = Si, Ge) compounds, the Mn sublattice orders magnetically in a wide temperature range while R sublattice shows magnetic ordering only at low temperature. The interlayer and intralayer Mn–Mn exchange interactions are very sensitive to the intralayer Mn–Mn distance (d^a_{Mn-Mn}). Roughly, if $d^a_{Mn-Mn} > 2.87$ Å ($a > 4.06$ Å), the intralayer (in-plane) Mn–Mn coupling is antiferromagnetic, while the interlayer (along *c*-axis) Mn–Mn coupling is ferromagnetic. In the case $2.84 < d^a_{Mn-Mn} < 2.87$ Å ($4.02 < a < 4.06$ Å), both the intralayer and interlayer couplings are antiferromagnetic. When $d^a_{Mn-Mn} < 2.84$ Å ($a < 4.02$ Å), there is no intralayer in-plane coupling, and the Mn sublattice is collinear ferromagnetic (light rare earth compound) or antiferromagnetic (heavy rare earth compound) along the *c*-axis [19–28].

Mössbauer spectroscopy [29], neutron scattering [30,31] and magnetization studies on single crystal [32] and polycrystal [30,33] show four magnetic phase transitions in $NdMn_2Ge_2$ compound. According to above references, various values of transition temperatures have been found for T_C(Nd) (21, 40, 100 K), T_{SR}(Mn) (210, 215, 250 K), T_C(Mn) (330, 334, 336, 339 K) and T_N(Mn) (415, 430 K).

* Corresponding author. Tel.: +86 01082648119; fax: +86 01082649084.
E-mail address: jluo@aphy.iphy.ac.cn (J. Luo).

0925-8388/$ – see front matter © 2009 Elsevier B.V. All rights reserved.
doi:10.1016/j.jallcom.2009.09.078

In this context, we report the effect of Fe substitution for Mn on the crystal structure, magnetic, and magnetocaloric properties of $Nd(Mn_{1-x}Fe_x)_2Ge_2$.

2. Experimental

The samples were prepared by arc-melting on a water-cooled copper crucible with a non-consumable tungsten electrode under high purity argon atmosphere. The purity of the elements was 99.98% for Mn and Fe, 99.9% for Nd, and 99.99% for Ge. To compensate the weight loss during melting and annealing, 10% excess of Mn was added before melting. The ingots were turned over and re-melted several times in order to achieve complete fusion and good homogeneity. The ingots were wrapped in Ta foil and annealed in an evacuated quartz tube at 900 °C for 2 weeks.

Crystal structure and phase identification of the samples were examined by X-ray powder diffraction (XRD). The XRD data were collected at room temperature using a Rigaku D/Max 2500 diffractometer with Cu Kα radiation and a graphite monochromator operated at 44 kV and 250 mA. The scan range was from 10° to 110° (2θ) with a step size of 0.02° and a sampling time of 1 s. The XRD profile fitting was performed using the DBWS9807a [34] program. The low temperature X-ray diffraction (LTXRD) studies were performed on the same diffractometer equipped with a low-temperature system. The temperature was controlled on an accuracy of about ±1 K with a PTC-20A temperature controller. The sample was heated to the desired temperature at a rate of 5 K/min and held for 5 min before recording the data. All measurements were carried out in a vacuum of about 2 Pa. The temperature dependence of the magnetization (M) of the samples was measured on a superconducting quantum interference device (SQUID) magnetometer at a low field (500 Oe) in the temperature range from 5 K to 300 K. The magnetization isothermals were measured by the SQUID magnetometer with magnetic fields up to 5 T at different temperatures. The specific heat of the samples was measured using a Modulated Differential Scanning Calorimeter (MDSC) (Q200, TA Instruments) in the temperature range of 200–370 K. The heating ramp was run at 5 K/min.

3. Results and discussion

Fig. 1 shows the Rietveld refinement results of the XRD data of $Nd(Mn_{0.9}Fe_{0.1})_2Ge_2$ at room temperature. Similar profile fitting was achieved for other compounds. The refinement shows that the compound is a single phase, crystallizing in the tetragonal $ThCr_2Si_2$-type structure belonging to the space group $I4/mmm$. The lattice

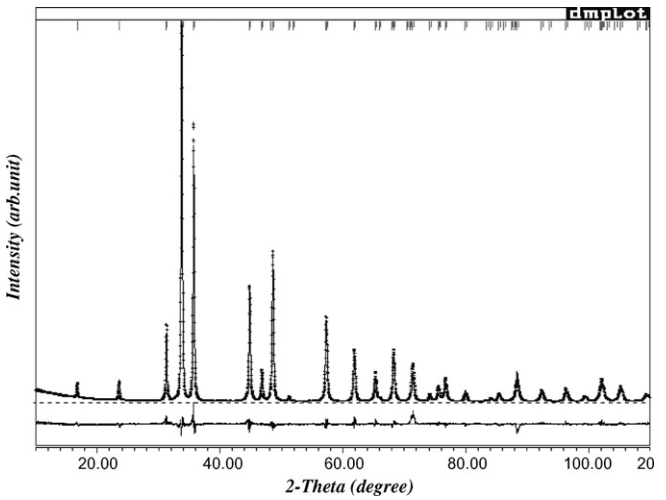

Fig. 1. The observed, calculated and residuals of the XRD of $Nd(Mn_{0.9}Fe_{0.1})_2Ge_2$. The small cross and continuous lines correspond to the experimental and calculated patterns respectively. The bottom curve depicts the difference between the experimental and calculated intensities.

constants a and c, and the unit-cell volume V derived from the XRD patterns are presented as a function of Fe concentration x in Fig. 2, and the values are listed in Table 1. Since the atomic radius of Fe is smaller than that of Mn, the substitution of Fe for Mn results in a decrease of the lattice constants a, c and the unit-cell volume V with increasing Fe content x. As a result, both the nearest intralayer Mn–Mn distance d^a_{Mn-Mn} and the nearest interlayer Mn–Mn distance d^c_{Mn-Mn} decrease with the Fe content (see Table 1).

The thermal variation of the magnetization for $x = 0.1$ and 0.2 compounds in an applied field of 500 Oe is presented in Fig. 3. For $x = 0.1$, a spin reorientation behavior is observed. The spin

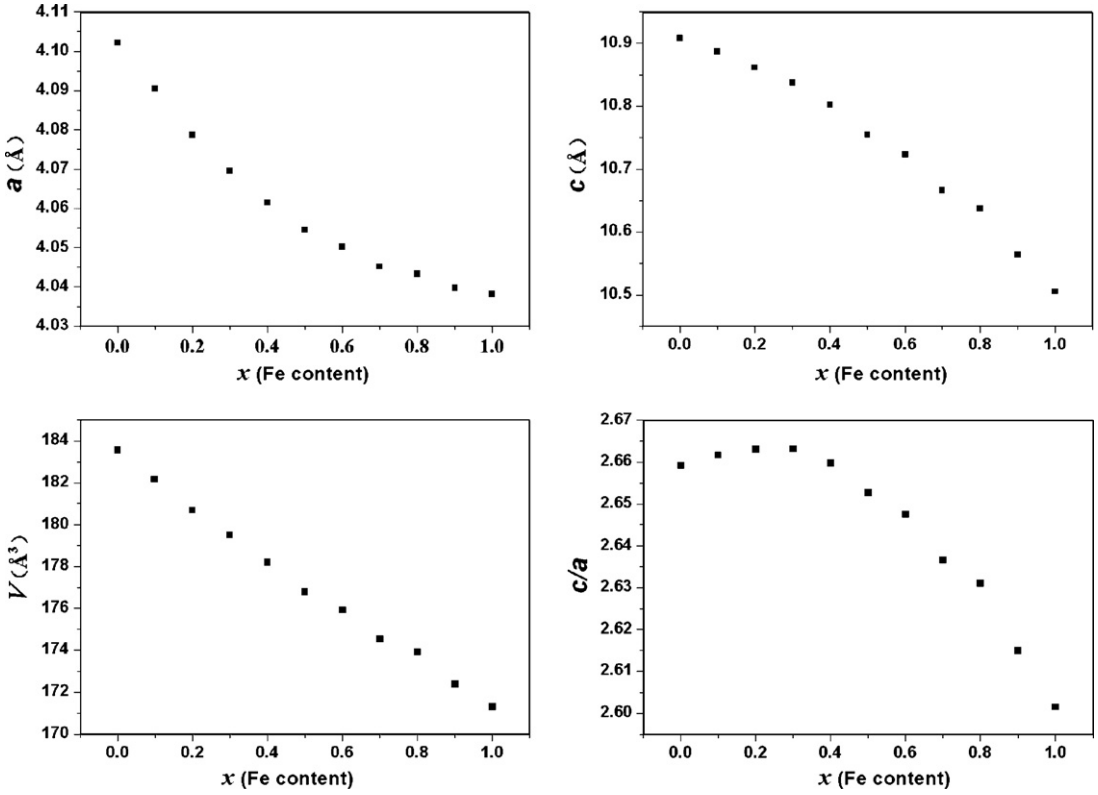

Fig. 2. The lattice constants a and c, unit cell V, and the c/a ratio of $Nd(Fe_xMn_{1-x})Ge_2$ as a function of Fe content x.

Table 1
The structural parameters derived from Rietveld refinements of the XRD patterns of $Nd(Fe_xMn_{1-x})_2Ge_2$ compounds.

x	a (Å)	c (Å)	V (Å^3)	c/a	d^a_{Mn-Mn}	Z (Ge site)	R_P (%)
0.0	4.1022(3)	10.9085(7)	183.57(4)	2.6592	2.9011	0.385	11.20
0.1	4.0905(2)	10.8876(5)	182.17(2)	2.6617	2.8929	0.384	10.58
0.2	4.0786(3)	10.8618(3)	180.68(3)	2.6631	2.8844	0.382	9.08
0.3	4.0695(1)	10.8376(2)	179.48(0)	2.6631	2.8780	0.382	9.45
0.4	4.0615(3)	10.8025(3)	178.19(1)	2.6597	2.8724	0.380	8.97
0.5	4.0545(3)	10.7548(1)	176.80(3)	2.6526	2.8674	0.381	9.77
0.6	4.0502(4)	10.7230(3)	175.90(5)	2.6475	2.8644	0.380	9.12
0.7	4.0452(0)	10.6657(6)	174.53(3)	2.6366	2.8608	0.378	8.72
0.8	4.0432(2)	10.6375(2)	173.90(1)	2.6310	2.8594	0.377	9.68
0.9	4.0397(2)	10.5639(3)	172.39(4)	2.6150	2.8569	0.377	8.68
1.0	4.0381(3)	10.5049(1)	171.30(3)	2.6015	2.8558	0.375	10.46

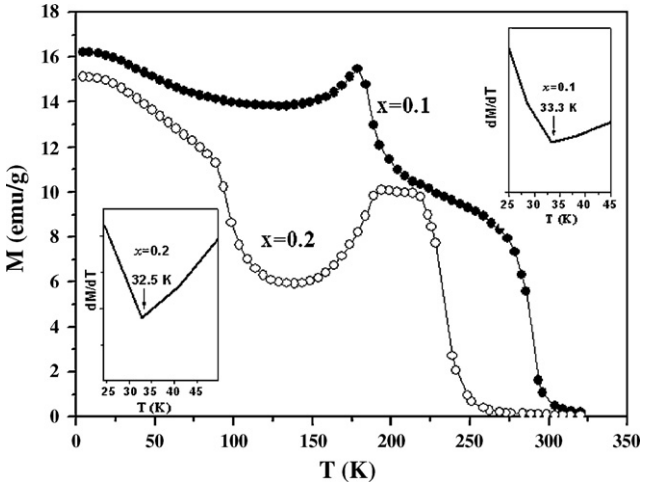

Fig. 3. Temperature dependence of the magnetization of $Nd(Fe_xMn_{1-x})Ge_2$ for $x = 0.1$ and 0.2 in a field of 500 Oe.

reorientation temperature (T_{SR} = 188 K) is determined by the cusp maximum of the $M(T)$ curve. Below T_{SR}, a weak transition is found at about 33.3 K (T_{Nd}), which is attributed to the ordering of the Nd sublattice [29–33]. Below T_{Nd}, the magnetization increases with decreasing temperature which could be explained by the ferromagnetic coupling of the Nd and Mn sublattices in this compound. The Curie temperature (T_C = 290 K) has been determined from the M^2–T curves by extrapolating M^2 to zero. For $x = 0.2$, the sample exhibits a $SmMn_2Ge_2$-like behaviour, characterized by four magnetic regions: above $T_{C1} \sim 235$ K, the sample is apparently paramagnetic; between 235 and 185 K, the sample behaves ferromagnetically; between $T_N \sim 185$ and 95 K, antiferromagnetism is observed; below $T_{C2} \sim 95$ K, ferromagnetic behaviour reappears. Below T_{C2}, a weak transition is also seen at about 32.5 K (T_{Nd}), which is similar to $x = 0.1$. It is noteworthy that a pure antiferromagnetic state is not reached in this compound, in contrast to $SmMn_2Ge_2$. As shown in Fig. 3, the magnetization M decreases with the increase of Fe content, which may be explained by magnetic dilution effect of the nonmagnetic Fe. (It is to note that the Fe atom is nonmagnetic in the RFe_2X_2 compounds. Even doped into the magnetic compound RMn_2X_2, Fe still behaves as a nonmagnetic element [35].) The substitution of Fe for Mn drastically influences the magnetic properties of the Mn sublattice and results in a fast decrease of T_C.

The LTXRD patterns of $Nd(Mn_{0.9}Fe_{0.1})_2Ge_2$ in the temperature range from 133 to 333 K is shown in Fig. 4 as an example, and no structural transition is observed. The shift of the Bragg position indicates that the lattice parameters and unit-cell volume of the compound vary with temperature, which are shown in Fig. 5 with the values listed in Table 2. In our measurement temperature range, d^a_{Mn-Mn} of $Nd(Mn_{0.9}Fe_{0.1})_2Ge_2$ is large than 2.87 Å ($a > 4.06$ Å). According to the previous report [19–28], for the $d^a_{Mn-Mn} > 2.87$ Å, the intralayer (in-plane) Mn–Mn coupling should be antiferromagnetic, while the interlayer (along c-axis) Mn–Mn coupling should be ferromagnetic. This agrees well with our magnetic measurement result. For $x = 0.2$, the d^a_{Mn-Mn} is very close to 2.87 Å between 133 and 183 K. As the references point out, the intralayer (in-plane) Mn–Mn coupling is antiferromagnetic, while the ferromagnetic and antiferromagnetic states coexist in the interlayer (along c-axis). This may explain why a pure antiferromagnetic state is not reached in this compound. When $T > 183$ K, the d^a_{Mn-Mn} is obviously large than 2.87 Å, so the interlayer (along c-axis) Mn–Mn coupling should be ferromagnetic, which also agrees well with our magnetic measurements.

Table 2
The values of lattice parameters and unit-cell volume at different temperatures for $Nd(Mn_{0.9}Fe_{0.1})_2Ge_2$ and $Nd(Mn_{0.8}Fe_{0.2})_2Ge_2$.

$x = 0.1$					$x = 0.2$				
T (K)	a (Å)	c (Å)	V (Å^3)	d^a_{Mn-Mn}	T (K)	a (Å)	c (Å)	V (Å^3)	d^a_{Mn-Mn}
133	4.0806(2)	10.8655(5)	180.92	2.886	133	4.0637(3)	10.8589(7)	179.32	2.873
153	4.0819(2)	10.8686(5)	181.09	2.887	153	4.0654(3)	10.8589(8)	179.47	2.874
173	4.0828(2)	10.8711(5)	181.22	2.887	173	4.0676(3)	10.8577(7)	179.65	2.876
183	4.0833(2)	10.8719(5)	181.27	2.888	183	4.0692(3)	10.8564(7)	179.77	2.877
193	4.0838(2)	10.8737(5)	181.35	2.888	193	4.0723(3)	10.8549(7)	179.93	2.880
203	4.0845(2)	10.8750(5)	181.43	2.889	203	4.0725(3)	10.8550(7)	180.03	2.880
213	4.0852(2)	10.8759(5)	181.50	2.889	223	4.0743(3)	10.8555(8)	180.20	2.881
223	4.0859(2)	10.8782(5)	181.61	2.890	233	4.0753(3)	10.8559(7)	180.30	2.882
243	4.0872(2)	10.8828(5)	181.80	2.891	243	4.0761(3)	10.8567(7)	180.38	2.882
263	4.0883(2)	10.8830(6)	181.90	2.891	253	4.0769(3)	10.8575(7)	180.47	2.883
273	4.0892(2)	10.8845(5)	182.01	2.892	263	4.0778(3)	10.8590(8)	180.57	2.884
283	4.0899(2)	10.8863(6)	182.09	2.892	283	4.0791(3)	10.8617(8)	180.73	2.885
293	4.0905(2)	10.8877(6)	182.17	2.893	300	4.0797(3)	10.8635(8)	180.81	2.885
300	4.0908(2)	10.8887(5)	182.22	2.893	323	4.0815(3)	10.8698(8)	181.08	2.886
313	4.0918(2)	10.8920(5)	182.36	2.894	343	4.0824(3)	10.8739(6)	181.22	2.887
333	4.0929(2)	10.8958(6)	182.52	2.895					

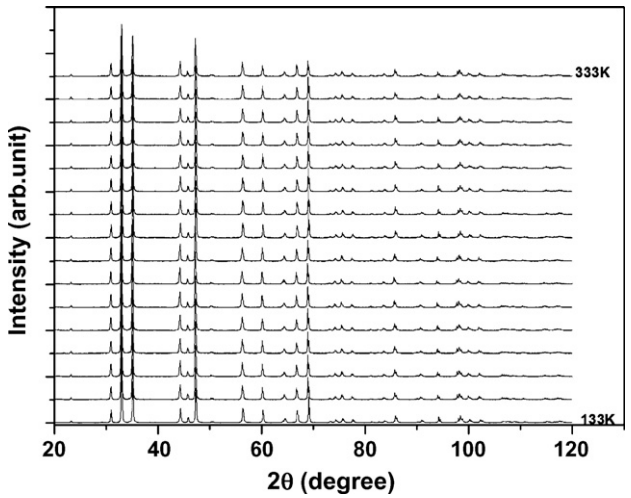

Fig. 4. LTXRD patterns of $Nd(Mn_{0.9}Fe_{0.1})_2Ge_2$ sample.

The magnetic isotherms of $Nd(Mn_{0.9}Fe_{0.1})_2Ge_2$ and $Nd(Mn_{0.8}Fe_{0.2})_2Ge_2$ compounds have been measured in the vicinity of the Curie temperature with the magnetic field from 0 to 5 T. As shown in Fig. 6, the magnetization increases rapidly at low field and shows a tendency to saturate with increasing field. It is well known that the magnetic transition can lead to the change of magnetic-entropy and the magnetocaloric effect can be characterized by isothermal magnetic entropy change. The Arrott plots are depicted in Fig. 7, which have been used to determine the type of phase transition of the sample near T_C according to the Inoue–Shimizu model [36]. This model involves a Landau expansion of the magnetic free energy (F) up to the sixth power of the total magnetization M,

$$F = \frac{C_1(T)}{2}M^2 + \frac{C_3(T)}{4}M^4 + \frac{C_5(T)}{6}M^6 - \mu_0 MH \quad (1)$$

It has been pointed out that the order of magnetic transition is closely related to the sign of the Landau coefficient $C_3(T)$ at the Curie temperature ($C_3(T_C)$) [37]. The magnetic transition is a first order when $C_3(T_C)$ is negative, whereas it is a second order for positive $C_3(T_C)$. The sign of $C_3(T_C)$ can be determined by means of the Arrott plots [38]. If the Arrott plot is S shaped near the magnetic transition temperature, $C_3(T_C)$ is negative; otherwise it is positive. As shown in Fig. 7, no S-shaped curve is exhibited near the Curie temperature. Therefore, the magnetic transition in $Nd(Mn_{1-x}Fe_x)_2Ge_2$ compounds is of second order.

The magnetic entropy change, ΔS, was calculated using Maxwell's thermodynamic relation $(\partial S/\partial H)_T = (\partial M/\partial T)_H$. The error of the calculated ΔS using this technique is within 3–10% [2]. The magnetic entropy change is given by

$$\Delta S_M(T,H) = S_M(T,H) - S_M(T,0) = \int_0^H \left(\frac{\partial S}{\partial H}\right) \mathrm{d}H$$

$$= \int_0^H \left(\frac{\partial M}{\partial T}\right) \mathrm{d}H \quad (2)$$

where H is the change of the applied field. For magnetization (M) measured at discrete field and temperature intervals, Eq. (2) can be approximated by the following expression [39]:

$$\Delta S = \sum_i \frac{1}{T_{i+1} - T_i}(M_{i+1} - M_i)_H \ \Delta H_i \quad (3)$$

where M_i and M_{i+1} are the magnetization values measured in a field H at temperatures T_i and T_{i+1}, respectively. The temperature dependence of the magnetic entropy changes of $Nd(Mn_{0.9}Fe_{0.1})_2Ge_2$ and

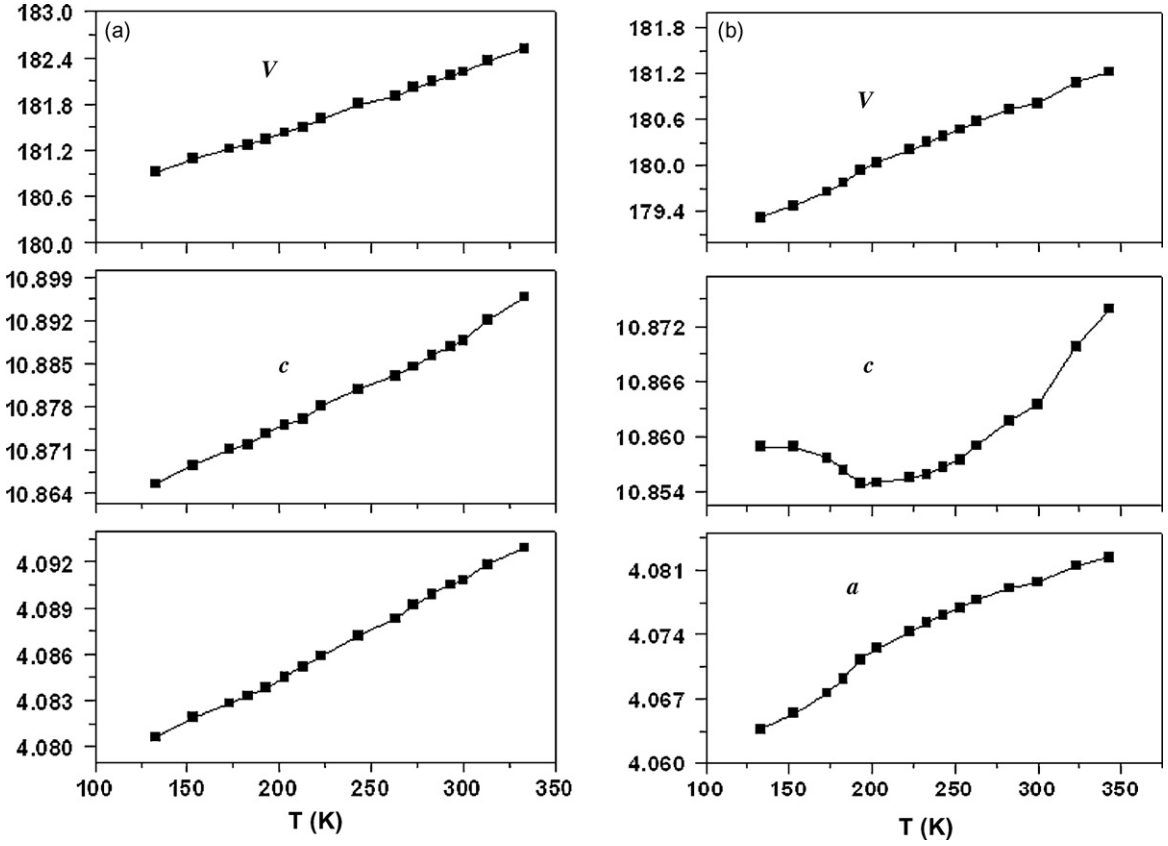

Fig. 5. The variation of lattice parameters and unit-cell volume with the temperature in (a) $Nd(Mn_{0.9}Fe_{0.1})_2Ge_2$ and (b) $Nd(Mn_{0.8}Fe_{0.2})_2Ge_2$.

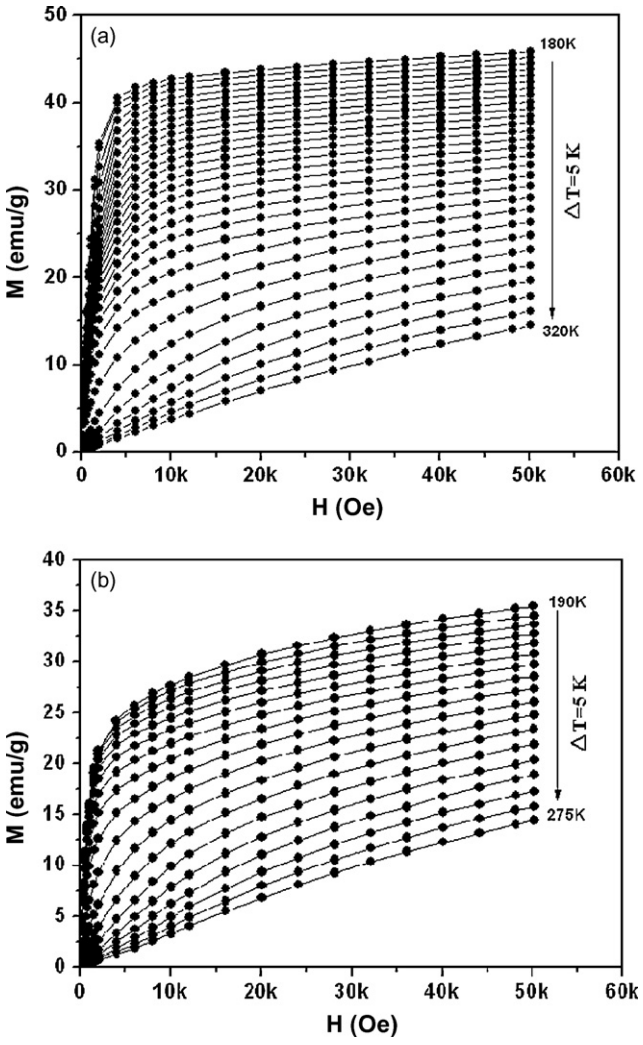

Fig. 6. Magnetization isotherms measured at different temperatures near T_C: (a) $Nd(Mn_{0.9}Fe_{0.1})_2Ge_2$ and (b) $Nd(Mn_{0.8}Fe_{0.2})_2Ge_2$.

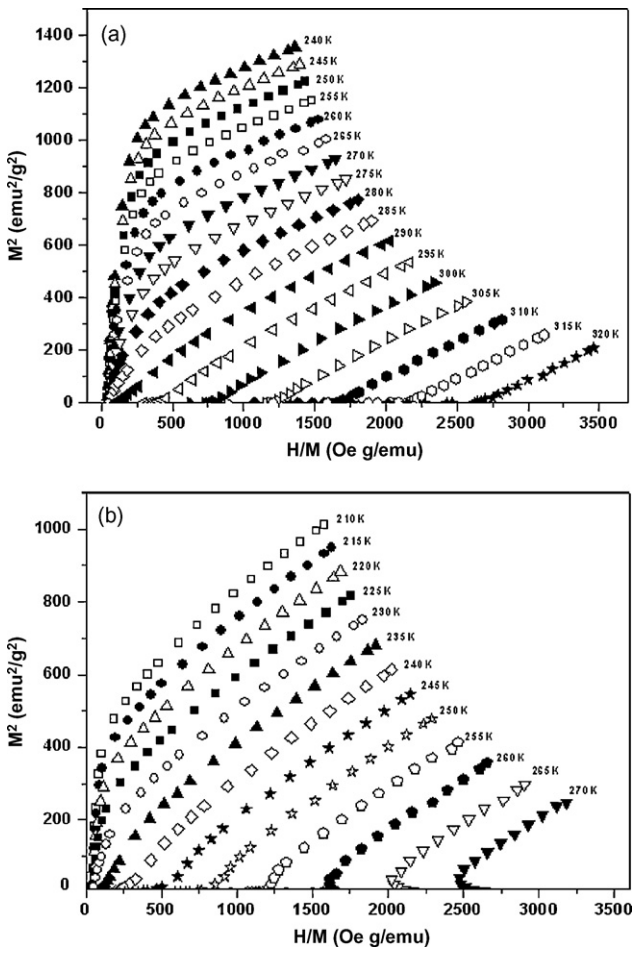

Fig. 7. Arrott plots at different temperatures near T_C: (a) $Nd(Mn_{0.9}Fe_{0.1})_2Ge_2$ and (b) $Nd(Mn_{0.8}Fe_{0.2})_2Ge_2$.

$Nd(Mn_{0.8}Fe_{0.2})_2Ge_2$, calculated from the isothermal magnetization curves by Eq. (3), is presented in Fig. 8 for different magnetic field changes of $\Delta H = 1$ T, 2 T, 3.2 T, 4 T and 5 T. The peak values are listed in Table 3. As shown in Fig. 8, the ΔS_M decreases gradually below the transition temperature, indicating a spreading distribution of ΔS_M. Therefore, despite the smaller magnitude of ΔS_M of the $Nd(Mn_{0.9}Fe_{0.1})_2Ge_2$ and $Nd(Mn_{0.8}Fe_{0.2})_2Ge_2$ compounds, their ΔS_M versus T curves are significantly broader. The ΔS_M^{max} values decrease with the iron content. On the one hand, the substitution of Fe for Mn results in a decrease of the magnetization moment due to the dilution effect of the nonmagnetic Fe. On the other hand, with the increase of iron content, the M–T curves become smooth.

Besides the magnitude of ΔS_M, there is another important characteristic parameter called relative cooling power (RCP), the amount of heat transferred in one thermodynamic cycle. According to the method of Gschneidner et al. [40], the RCP value for reversible refrigeration was obtained by numerically integrating the area under the ΔS_M versus T curve, using the temperature at half maximum of the ΔS_M peak as the integration limit:

$$\mathrm{RCP} = \int_{T_{cold}}^{T_{hot}} \Delta S_M(T)\, \mathrm{d}T, \tag{4}$$

where T_{hot} and T_{cold} are the corresponding two temperatures of half maximum of the ΔS_M peak. δT_{FWHM} is the difference between T_{hot} and T_{cold}:

$$\delta T_{FWHM} = T_{hot} - T_{cold} \tag{5}$$

The RCP values for $Nd(Mn_{0.9}Fe_{0.1})_2Ge_2$ and $Nd(Mn_{0.8}Fe_{0.2})_2Ge_2$ are listed in Table 4.

Table 3
The peak values of isothermal magnetic entropy change at different applied field.

	H (T)				
	1	2	3.2	4	5
$x = 0.1$					
ΔS_M (J/kg K)	0.63	1.17	1.68	1.98	2.35
$x = 0.2$					
ΔS_M (J/kg K)	0.53	0.93	1.32	1.57	1.84

Table 4
The magnetocaloric parameters of $Nd(Mn_{0.9}Fe_{0.1})_2Ge_2$ and $Nd(Mn_{0.8}Fe_{0.2})_2Ge_2$ compounds.

	ΔH (T)				
	1	2	3.2	4	5
$x = 0.1$					
RCP (J/kg)	18.4	46.1	86.4	112.7	145.9
δT_{FWHM} (K)	29.2	39.4	51.4	56.9	62.1
$x = 0.2$					
RCP (J/kg)	18.6	44.1	77.4	102.2	133.8
δT_{FWHM} (K)	35.0	47.4	58.6	65.1	72.7

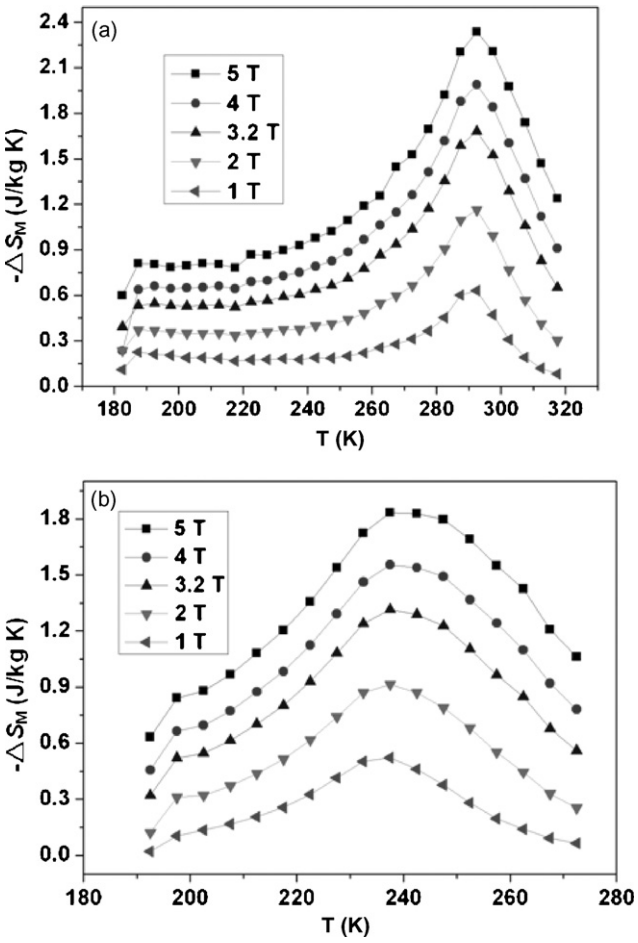

Fig. 8. Temperature dependence of the isothermal magnetic entropy change under different applied magnetic field: (a) $Nd(Mn_{0.9}Fe_{0.1})_2Ge_2$ and (b) $Nd(Mn_{0.8}Fe_{0.2})_2Ge_2$.

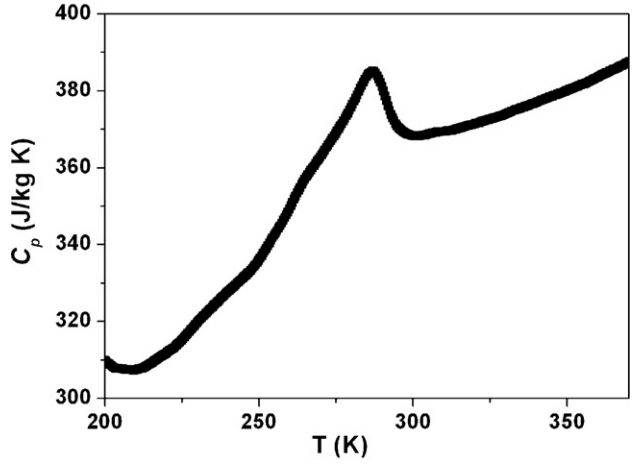

Fig. 9. The heat capacity C_P of $Nd(Mn_{0.9}Fe_{0.1})_2Ge_2$ between 200 and 370 K.

The temperature dependence of the specific heat C_P of $Nd(Mn_{0.9}Fe_{0.1})_2Ge_2$ is shown in Fig. 9. The λ-shape maximum on the specific heat curve at 287 K agrees with the Curie temperature T_C of this compound determined by the magnetic measurement. The shape of the peak is typical for a second-order phase transition, which is in accordance with the result determined by Arrott plot.

4. Conclusions

We have studied the effect of Fe substitution on the structural, magnetic, and magnetocaloric of $Nd(Mn_{1-x}Fe_x)_2Ge_2$. The results presented in this work indicate that in the $Nd(Mn_{1-x}Fe_x)_2Ge_2$ system the crystal structure remains unchanged upon Fe substitution, but the lattice constant decreases with the Fe concentration. The change in the lattice parameters, obtained from the LTXRD, is found to be correlated with the magnetic properties. The substitution of iron drastically influences the magnetic properties of the Mn sublattice and results in a fast decrease of T_C. The behavior of the magnetization in the vicinity of the Curie temperature reveals the second-order character of the phase transition. The admixture of the Fe atoms does not influence the magnetic ordering in the Nd-sublattice, but only leads to a small change of the T_R. The Mn-sublattice exhibits a magnetic ordering in the wide temperature range. There is a spin reorientation for $x = 0.1$ as previously reported in $NdMn_2Ge_2$ and it disappears with iron addition. A ferro-antiferromagnetic transition is observed in the $Nd(Mn_{0.8}Fe_{0.2})_2Ge_2$ compound. However, a pure antiferromagnetic state is not reached in this compound. The maximum values of ΔS_M are found to be 2.35 and 1.84 J/kg K for $x = 0.1$ and 0.2 under the applied field change from 0 T to 5 T. The ΔS_M^{max} values decrease with the iron content since the magnetization moment decreases due to the dilution effect of the nonmagnetic Fe and the M–T curves become smoother for $x = 0.2$. The relative cooling power (RCP) of $Nd(Mn_{0.9}Fe_{0.1})_2Ge_2$ and $Nd(Mn_{0.8}Fe_{0.2})_2Ge_2$ is 145.9 and 133.8 J kg^{-1} under an applied field change of 5 T.

Acknowledgement

This work was supported by the National Basic Research Program of China (Grant No. 2006CB601101).

References

[1] K.A. Gschneidner Jr., V.K. Pecharsky, A.O. Tsokol, Rep. Prog. Phys. 68 (2005) 1479.
[2] V.K. Pecharsky, K.A. Gschneidner Jr., J. Magn. Magn. Mater. 200 (1999) 44.
[3] H. Wada, T. Morikawa, K. Taniguchi, T. Shibata, Y. Yamada, Y. Akishige, Phys. B 328 (2003) 114.
[4] O. Tegus, E. Brück, K.H.J. Buschow, F.R. de Boer, Nature 415 (2002) 150.
[5] E. Brück, O. Tegus, X.W. Li, F.R. de Boer, K.H.J. Buschow, Phys. B 327 (2003) 431.
[6] E. Warbury, Ann. Phys. 13 (1881) 141.
[7] V.K. Pecharsky, K.A. Gschneidner Jr., Phys. Rev. Lett. 78 (1997) 4494.
[8] H. Wada, Y. Tanabe, Appl. Phys. Lett. 79 (2001) 3302.
[9] A. Fujita, S. Fujieda, Y. Hasegawa, K. Fukamichi, Phys. Rev. B 67 (2003) 104416.
[10] S. Gama, A.A. Coelho, A. de Campos, A. Magnus, G. Carvalho, F.C.G. Gandra, P.J. von Ranke, N.A. de Oliveira, Phys. Rev. Lett. 93 (2003) 237202.
[11] P.J. von Ranke, N.A. de Oliveira, S. Gama, J. Magn. Magn. Mater. 277 (2004) 78.
[12] N.A. de Oliveira, Eur. Phys. J. B 40 (2004) 259.
[13] N.A. de Oliveira, P.J. von Ranke, J. Phys.: Condens. Matter. 17 (2005) 3325.
[14] I. Dincer, A. Elmali, Y. Elerman, J. Alloys Compd. 385 (2004) 59.
[15] S. Kervan, Y. Elarman, M. Acet, Solid State Commun. 119 (2001) 95.
[16] T. Fujiwara, H. Fujii, T. Shigeoka, Phys. Rev. B 63 (2001) 17440.
[17] J.H.V.J. Brabers, A.J. Nolten, F. Kayzel, S.H.J. Lenczowaki, K.H.J. Buschow, F.R. de Boer, Phys. Rev. B 50 (1994) 16410.
[18] Z. Ban, M. Sikirica, Acta Crystallogr. 18 (1965) 594.
[19] S. Kervan, Y. Elerman, M. Acet, J. Alloy Compd. 335 (2002) 70–76.
[20] A. Kilic, S. Kervan, Ş. Özcan, A. Gencer, J. Magn. Magn. Mater. 288 (2005) 244–249.
[21] S. Kervan, Y. Elerman, M. Acet, J. Alloy Compd. 321 (2001) 35–39.
[22] G. Venturini, R. Welter, E. Ressouche, B. Malaman, J. Alloy Compd. 224 (1995) 262–268.
[23] G. Venturini, J. Alloy Compd. 232 (1996) 133–141.
[24] M.N. Norlidah, G. Venturini, B. Malaman, E. Ressouche, J. Alloy Compd. 245 (1996) 80–88.
[25] M.N. Norlidah, G. Venturini, B. Malaman, E. Ressouche, J. Alloy Compd. 248 (1997) 112–120.
[26] G. Venturini, R. Welter, E. Ressouche, B. Malaman, J. Alloy Compd. 223 (1995) 101–110.
[27] G. Venturini, R. Welter, E. Ressouche, B. Malaman, J. Magn. Magn. Mater. 150 (1995) 197–212.
[28] P. Kumar, N.K. Singh, K.G. Suresh, A.K. Nigam, S.K. Malik, J. Appl. Phys. 101 (2007) 013908.

[29] I. Nowik, Y. Levi, I. Felner, E.R. Bauminger, J. Magn. Magn. Mater. 147 (1995) 373.
[30] R. Welter, G. Venturini, E. Ressouche, B. Malaman, J. Alloy Compd. 218 (1995) 204.
[31] L. Morellon, P.A. Algarabel, M.R. Ibarra, Phys. Rev. B 55 (1997) 12363.
[32] T. Shigeoka, N. Iwata, H. Fuji, J. Magn. Magn. Mater. 76 and 77 (1988) 189.
[33] Y.G. Wang, F. Yang, C. Chen, N. Tang, Q. Wang, Phys. Status Solidi (a) 162 (1997) 723.
[34] R.A. Young, A.C. Larson, C.O. Paiva-Santos, User's Guide to Program DBWS-9807a for Rietveld Analysis of X-ray and Neutron Powder Diffraction Patterns with a PC and Various Other Computers, School of Physics, Georgia Institute of Technology, Atlanta, Georgia, 1999.
[35] I. Nowik, Y. Levi, I. Felner, E.R. Bauminger, J. Magn. Magn. Mater. 147 (1995) 373–384.
[36] J. Inoue, M. Shimizu, J. Phys. F: Met. Phys. 12 (1982) 1811.
[37] X.B. Liu, Z. Altounian, J. Magn. Magn. Mater. 292 (2005) 83.
[38] N.H. Duc, D.T. Kim Anh, P.E. Brommer, Phys. B 319 (2002) 1.
[39] M. Földeàki, R. Chahine, T.K. Bose, J. Appl. Phys. 77 (1995) 3528.
[40] K.A. Gschneidner Jr., V.K. Pecharsky, A.O. Pecharshy, C.B. Zimm, Mater. Sci. Forum 315–317 (1999) 69.